Journal of Molecular Structure 1282 (2023) 135227

Contents lists available at ScienceDirect

Journal of Molecular Structure

journal homepage: www.elsevier.com/locate/molstr

Cooperativity effects in a new pterostilbene/phenanthroline cocrystal

Rafael Barbas[a], Lídia Bofill[b], Vineet Kumar[b], Rafel Prohens[a,b,*], Antonio Frontera[c,**]

[a] Unitat de Polimorfisme i Calorimetria, Centres Científics i Tecnològics, Universitat de Barcelona, Baldiri Reixac 10, 08028 Barcelona, Spain
[b] CIRCE Scientific, Parc Científic de Barcelona, Baldiri Reixac 4-12, 08028 Barcelona, Spain
[c] Departament de Química, Universitat de les Illes Balears, Crta. de Valldemossa km 7.5, 07122 Palma, Spain

ARTICLE INFO

Article history:
Received 22 November 2022
Revised 9 January 2023
Accepted 23 February 2023
Available online 24 February 2023

Keywords:
Nutraceuticals
Pterostilbene
Hirshfeld surfaces
Cocrystal
MEPS
NCIPlot
QTAIM

ABSTRACT

The SCXRD structure of the natural dietary compound pterostilbene (trans-3,5-dimethoxy-4-hydroxystilbene) and phenanthroline (1,10-phenanthroline) cocrystal is reported herein. In the solid state the cocrystal forms several H-bonded and C–H···π supramolecular synthons that have been analyzed by DFT calculations, with a particular focus on the parallel face-to-face stacking of the phenanthroline rings, a relevant and quite unusual feature (antiparallel displaced mode is more common). Cooperativity effects between H-bonding and aromatic interactions have been studied to rationalize the formation of this unusual π-stacking mode and the supramolecular assemblies have been further analyzed using several computational techniques, i.e., molecular electrostatic potential (MEP) surfaces and the quantum theory of "atom-in-molecules" (QTAIM) combined with reduced density gradient (RDG) plots.

1. Introduction

Multicomponent crystal forms of nutraceutical and pharmaceutical ingredients have attracted the attention of researchers from both academic and industrial areas because the originally promising properties envisioned by the pioneering work of renowned crystal engineers have become today real [1]. The huge corpus of crystallographic data that hundreds of cocrystals have generated has allowed to understand better how two or more different compounds pack together in a single solid phase through a rich combination of weak intermolecular interactions [2]. However, there is still the need for a deeper understanding of such forces in order to, on the one hand predict the formation of cocrystals, and on the other hand their structural features. In this sense, aromatic interactions [3], present ubiquitously in organic crystalline materials, although much weaker than hydrogen bonds (mostly used for the engineering of new cocrystals) are capable of driving the formation of a particular packing pattern [4] and at the same time be influenced by the presence of other forces in the crystal [5].

In this work, we have computational and crystallographically analyzed a new cocrystal formed by pterostilbene and phenanthroline (Fig. 1) and studied the interplay of aromatic interactions and hydrogen bonds related to the parallel orientation of the molecular dipoles shown by the phenanthroline molecules. In the solid state, both molecules are connected via OH···N H-bonds and CH···π interactions. Moreover, the solid state architecture of the cocrystal shows an almost perfect face-to-face parallel stacking of the phenanthroline rings. Such binding mode is not common, since the antiparallel orientation of the molecular dipoles is energetically favoured with respect to the parallel orientation, as demonstrated before. The assemblies observed in the solid state have been studied using density functional theory (DFT) calculations in combination with molecular electrostatic potential (MEP) surfaces, noncovalent interaction plot (NCIPlot) and the quantum theory of "atom-in-molecules" (QTAIM) focusing on the H-bonding, π-stacking, and CH···π interactions.

2. Experimental section

2.1. Materials

Phenanthroline was purchased from Sigma-Aldrich and used without further purification. Pterostilbene was purchased from Dynveo and purified following the procedure described in reference [6]. Single crystals suitable for SXCRD analysis was obtained

* Corresponding author at: Unitat de Polimorfisme i Calorimetria, Centres Científics i Tecnològics, Universitat de Barcelona, Baldiri Reixac 10, 08028 Barcelona, Spain.
** Co-corresponding author. Departament de Química, Universitat de les Illes Balears, Crta. de Valldemossa km 7.5, 07122 Palma, Spain.
E-mail addresses: rafel@ccit.ub.edu (R. Prohens), toni.frontera@uib.es (A. Frontera).

https://doi.org/10.1016/j.molstruc.2023.135227

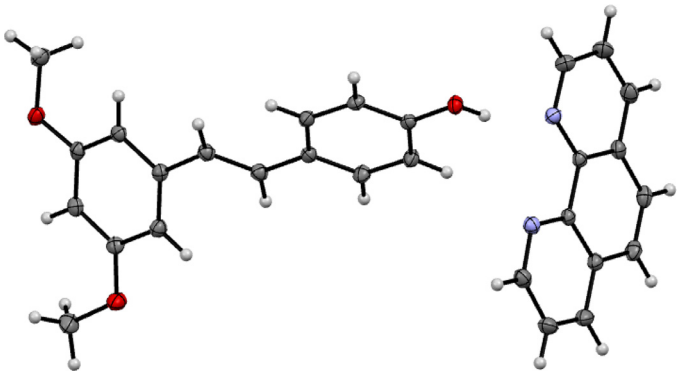

Fig. 1. ORTEP representation of the asymmetric unit of the pterostilbene/phenanthroline cocrystal.

Table 1
Crystal data of the pterostilbene/phenanthroline cocrystal.

Crystal form	Pterostilbene:Phenanthroline
Empirical formula	$C_{28}H_{24}N_2O_3$
Formula weight	436.49
Temperature (K)	100(2)
Crystal system	Monoclinic
Space group	*C*2/*c*
a (Å)	25.0336(10)
b (Å	10.0532(4)
c (Å)	18.3403(6)
α (°)	90
β (°)	105.492(2)
γ (°)	90
Volume (Å^3)	4448.0(3)
Z	8
Density (calc. (Mg/m^3)	1.304
Final R indices [$I > 2\sigma(I)$]	R1=0.0433, wR2=0.1072
CCDC	2,214,987

as follows. Pterostilbene (50 mg, 0.195 mmol) and phenanthroline (35.5 mg, 0.196 mmol) were dissolved together in methyl isobutyl ketone (0.3 mL) at 25 °C and stored sealed. Single crystals were observed after 7 days.

2.2. X-Ray data collection

Single crystal X-ray diffraction (SCXRD) intensity data of the pterostilbene/phenanthroline cocrystal was collected using a D8 Venture system equipped with a multilayer monochromator and a Mo microfocus ($\lambda = 0.71073$ Å). Frames were integrated with the Bruker SAINT software package using a SAINT algorithm. Data were corrected for absorption effects using the multi-scan method (SADABS) [7]. The structure was solved and refined using the Bruker SHELXTL Software Package, a computer program for automatic solution of crystal structures and refined by full-matrix least-squares method with ShelXle Version 4.8.0, a Qt graphical user interface for SHELXL computer program [8]. Table 1 contains the crystallographic data for the structure.

2.3. DFT calculations

The density functional theory study of the supramolecular synthons observed in the solid state of the pterostilbene /phenanthroline cocrystal was done using the Gaussian-16 [9] program and the PBE0-D3/def2-TZVP level of theory [10,11]. The interaction energies of the assemblies were estimated by calculating the difference between the absolute energies of isolated monomers and their assembly. In this manuscript, the BSSE (basis set superposition error) correction was considered and, consequently, the reported interaction energies were corrected using the Boys-Bernardi [12] methodology. This level of theory has been chosen because previous studies have demonstrated its suitability to describe the noncovalent interactions described herein [13–16]. Further characterization of the noncovalent contacts observed in the pterostilbene /phenanthroline cocrystal was performed by using the Bader's "Atoms in molecules" theory (QTAIM) [17]. These calculations were carried out using the AIMAll calculation package [18]. The noncovalent interaction plot (NCIplot) [19] by means of plotting the reduced density gradient (RGD) isosurfaces has been used to reveal the noncovalent interactions in real space. The MEP surface plots were generated using the Gaussian-16 software [9] and the 0.001 a.u. isovalue for the density as a best estimate of the van der Waals envelop.

3. Results and discussion

3.1. Structural description

A colorless prism single crystals of the pterostilbene/phenantroline cocrystal suitable for SXRD analysis were obtained in methyl isobutyl ketone. The crystal structure reveals a monoclinic cell in the *C*2/*c* space group with one molecule of each component in the asymmetric unit (Z'=1, $Z = 8$). The asymmetric unit with ORTEP representation is shown in Fig. 1 and the crystallographic data and structural refinements details are summarized in Table 1.

We have determined the Hirshfeld surfaces [20] and the associated fingerprint plot [21,22] of each molecule by using the Crystal Explorer software [23] (Fig. 2) and their analysis reveal that expected strong H-bonds between the phenol OH and the nitrogen atoms of phenanthroline are formed together with a relevant contribution of aromatic interactions (π-stacking and CH$\cdots\pi$, detected as C···C and C···H contacts on the fingerprint plot).

The most relevant structural feature is that the three aromatic rings of the phenanthroline molecules are face-to-face stacked in a dipole-dipole parallel orientation with all distances between centroids equal to 3.7 Angstroms (Fig. 3). These contacts count for the 10.1% of the contacts for the phenanthroline molecule in the fingerprint plot.

In order to analyze the trend of phenanthroline to establish π-stacking interactions in the solid state we have conducted a search in the CSD (version 5.41, November 2019) using ConQuest 2.0.2. Certain restrictions were applied during the search, thus only structures with 3D coordinates determined were included, the R factor was set to be less than 10%, structures with disorder and errors, as well as polymeric, organometallic and powder structures were excluded from the analysis. 178 crystal structures containing phenanthroline in a non-protonated form were found under these restrictions and we applied a qualitative criterion for a rough estimate of the stacking tendency. As we were only interested in detecting the trend and not in a genuine statistical analysis, visual inspection of the phenanthroline molecules was followed to label as stacked those structures with a partial horizontal overlap of aromatic surfaces and non-stacked otherwise. Moreover, the parallel or antiparallel orientation was also assessed qualitatively by visual inspection. ESI section contains a table with this assessment, which reveals that the antiparallel orientation of dipoles in phenanthroline is the preferred one (56%), with a non-negligible number of structures not showing staked assemblies (25%) and only 20% of the structures showing parallel orientation, as expected since dipoles maximize the interaction energy if anti-paralleled oriented because according to electrostatic theory, which states that the interaction energy of two parallel dipoles should be proportional to the magnitude of their dipole moment vectors and the cosine of their vector angles [24]. Thus, in order to get deeper insight into

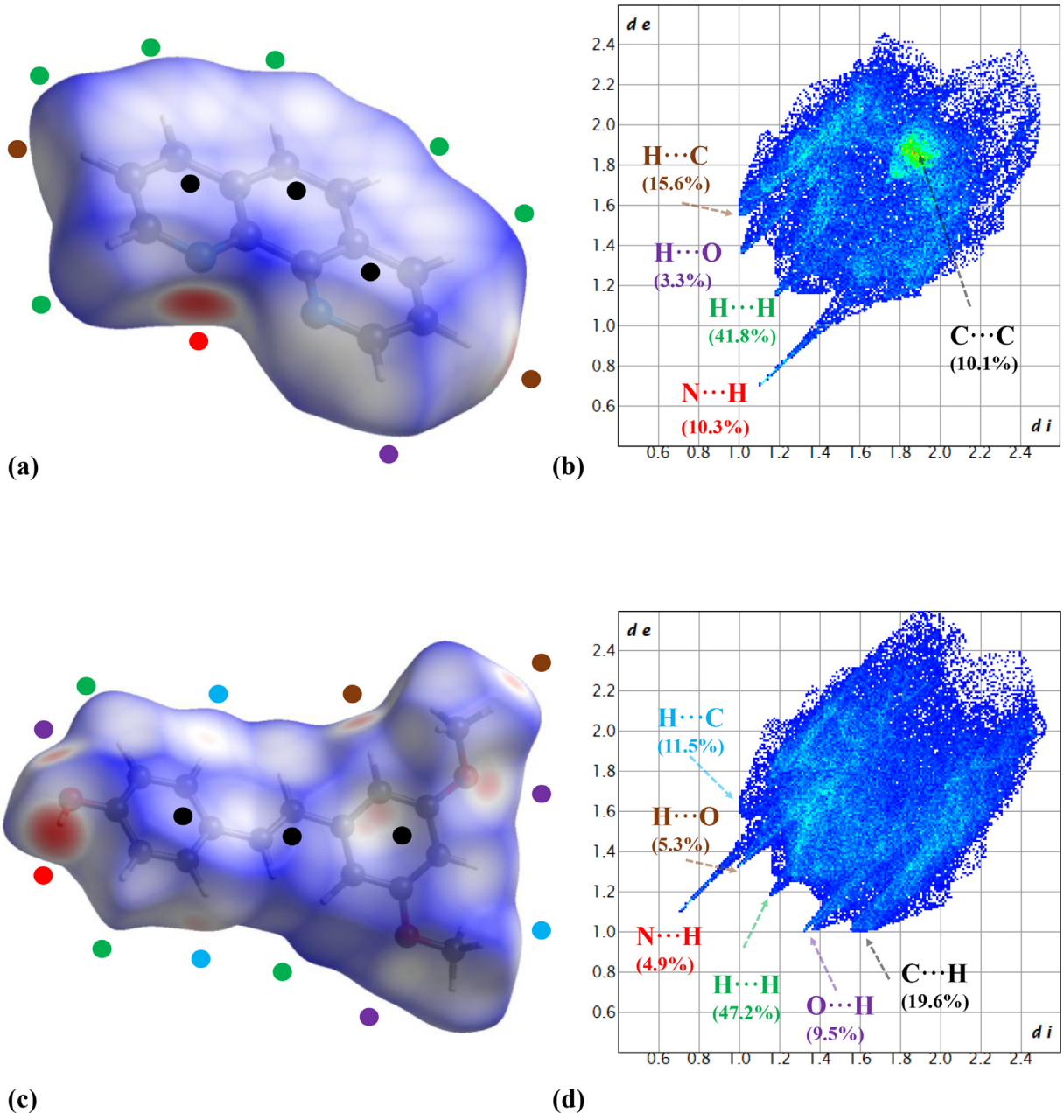

Fig. 2. (a, c) Hirshfeld surfaces mapped with d_{norm} (a, c) and Fingerprint plots computed from Hirshfeld surfaces (b, d) for phenanthroline and pterostilbene molecules respectively. Each type of contact is highlighted in colours on the corresponding regions of the Hirshfeld surfaces and their surface area contribution (%) of intermolecular contacts are also represented.

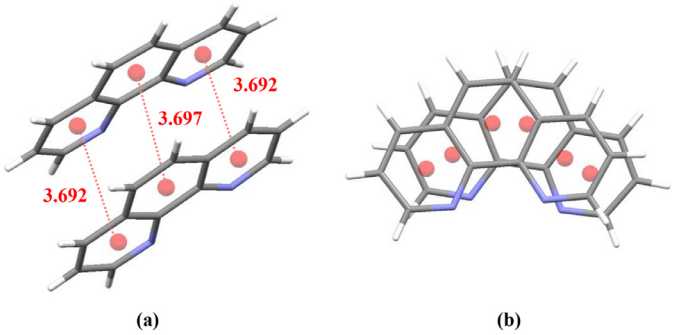

Fig. 3. (a) Distances between centroids in the phenanthroline parallel assembly. Centroids distances in Å. (b) Representation of the phenanthroline face-to-face stacking in a zenith view.

the forces responsible for stabilizing the unstable parallel stacking we have devoted the main part of this work to the computational analysis of the energetics associated to the main intermolecular interactions in the cocrystal.

3.2. DFT calculations of the supramolecular assemblies

The DFT study of supramolecular assemblies is essentially focused on the parallel face-to-face stacking of the phenanthroline rings shown in Fig. 4 and the influence of the appended pterostilbene molecules on the π-stacking. In particular, two pterostilbene molecules form strong OH···N bonds with the phenanthroline π-stacked dimer and the other two form $CH_3\cdots\pi$ interactions. Such contacts likely reinforce the parallel π-stacking interaction, as analyzed in the following sections.

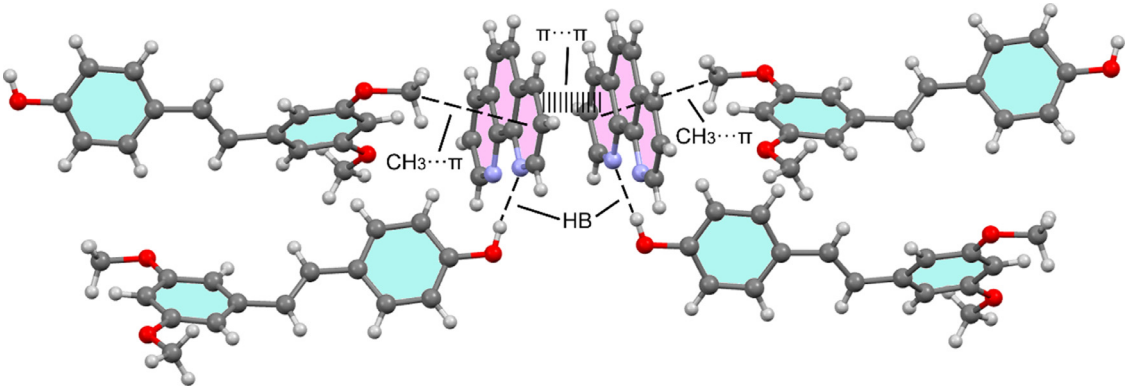

Fig. 4. Partial view of the cocrystal showing the π-staked dimer of phenanthroline and four appended pterostilbene molecules via hydrogen bonds and CH···π interactions.

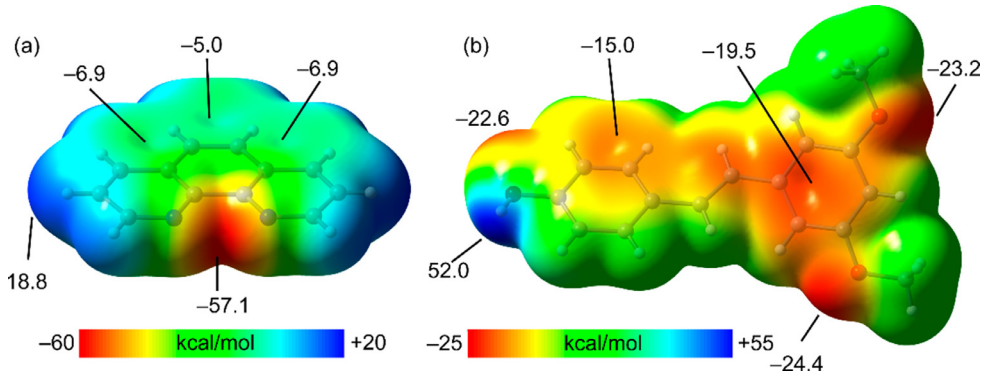

Fig. 5. MEP surfaces of phenanthroline (a) and pterostilbene (b) at the PBE0-D3/def2-TZVP level of theory (density isovalue 0.001 a.u.). MEP energies in kcal/mol.

3.2.1. MEP study

Initially, the MEP surface plots of the coformers were represented (see Fig. 5) to investigate the most nucleophillic and electrophilic parts of the molecules and rationalize the interactions represented in Fig. 4. For phenanthroline (Fig. 5a), the MEP minimum (–57.1 kcal/mol) is located at the region under the influence of both N-atoms, as expected. The MEP values are also negative over the aromatic rings (–5.0 kcal/mol over the central ring and –6.9 kcal/mol over the other two). Such small MEP values explain the strong ability to stack, since the electrostatic repulsion is easily compensated by other forces like dispersion. The MEP values are positive at the aromatic H-atoms (18.8 kcal/mol). For pterostilbene (Fig. 5b), the MEP minima is located at the O-atoms of the methoxyl groups (–23.2 and –24.4 kcal/mol) and the maximum MEP is found at the phenolic OH (+52.0 kcal/mol). The MEP values are negative over the aromatic rings. Considering both co-formers together, the MEP maximum is found in the phenanthroline molecule and the minimum at the pterostilbene, thus the most favored interaction between both co-formers corresponds to OH···N(amide) that is actually found in the assembly shown in Fig. 4.

The MEP analysis has been also used to study the effect of the H-bonds and $CH_3\cdots\pi$ interaction on the electronic nature of the phenanthroline molecule to further rationalize the formation of the unusual face-to-face parallel stacking. To do so, we have computed the MEP surface of the H-bonded and $CH_3\cdots\pi$ dimers, that are represented in Fig. 6. In addition, we have also computed the MEP surface of the phenanthroline π-stacked dimer (Fig. 6a) to explore the possible increase in the basicity of the N-atoms of phenanthroline. Interestingly, the MEP value at the N-atom increases in the dimer to –60.7 kcal/mol, with respect to the monomer, thus demonstrating that the H-bond acceptor ability of phenanthroline increases upon formation of the dimer. Also interestingly, in the dimer where the phenanthroline and the pterostilbene are held together by the H-bond (see Fig. 6b), the MEP over the center of the ring decreases, becoming almost electroneutral. This explains the formation of face-to-face dimers in the solid state, since the electrostatic repulsion is negligible between the aromatic rings and the dispersion force is maximized in this conformation. Finally, the $CH_3\cdots\pi$ dimer has a minimum effect on the MEP values at the phenanthroline ring, with a small MEP reduction over the central ring. This result suggests the existence of synergetic effects between the π-stacking and H-bonding interactions in the solid state of the cocrystal.

3.2.2. QTAIM and energetic study

The QTAIM distribution analyses of several assemblies of the cocrystals are provided in Fig. 7, along with the binding energies. The phenanthroline π-stacked homodimer is represented in Fig. 7a, evidencing the existence of three bond critical points (CPs) and bond paths connecting both molecules. Moreover, an extended green reduced density gradient (RDG) isosurface is located between the aromatic rings, embracing the whole π-systems, confirming the large overlap of the π-clouds. The binding energy this self-assembled dimer is –5.9 kcal/mol. The QTAIM of the H-bonded heterodimer is shown in Fig. 7b, disclosing that the OH···N is characterized by a bond CP and bond path connecting the H-atom to one N-atom of phenantroline. A blue RDG isosurface is also observed coincident with the bond CP, indicating the strong nature of this H-bond (the color code used herein is green for weak and blue for strong NCIs). The analysis also evidences the existence of a secondary H-bond that is formed between one aromatic CH bond and the other N-atom of phenanthroline. This H-bond is also characterized by the corresponding bond CP, bond path and green RDG isosurface. The binding energy of this heterodimer is –10.9 kcal/mol, stronger that the π-stacking homod-

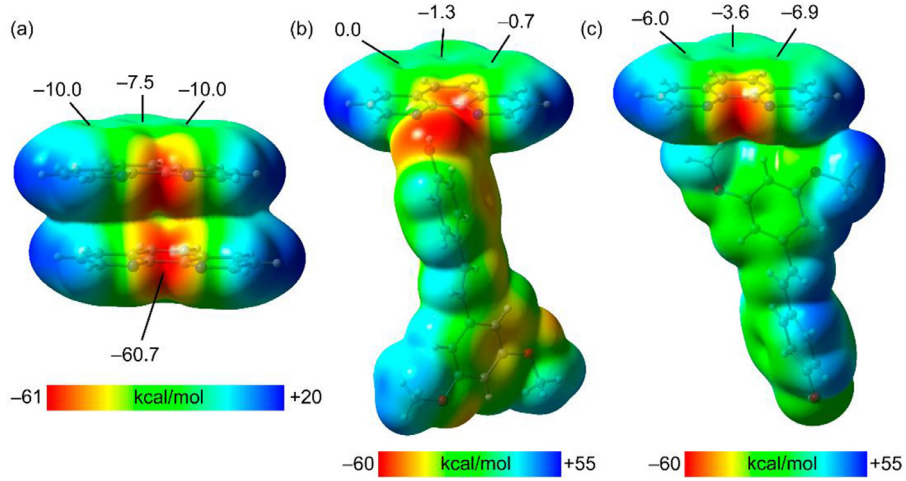

Fig. 6. MEP surfaces of phenanthroline dimer (a), pterostilbene/phenanthroline H-bonded dimer (b) and pterostilbene/phenanthroline CH_3–π dimer (c) at the PBE0-D3/def2-TZVP level of theory (density isovalue 0.001 a.u.). MEP energies in kcal/mol.

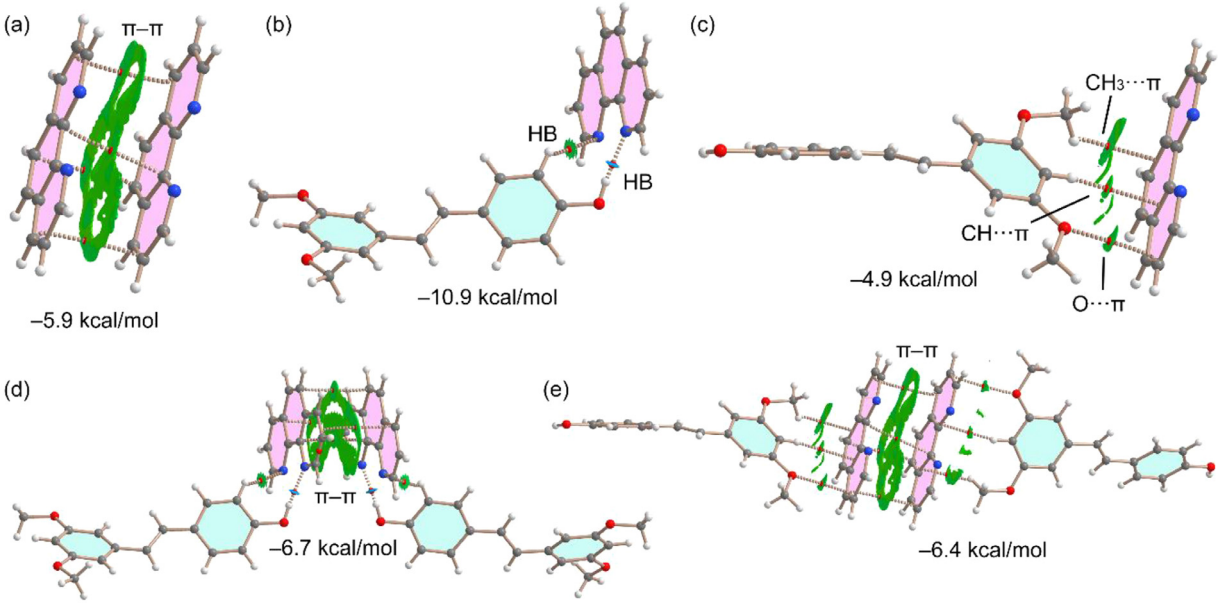

Fig. 7. QTAIM analysis of intermolecular bond CPs (red spheres) and bond paths for the homodimer (a), heterodimers (b,c) and tetramers (d,e) observed in the pterostilbene/phenanthroline cocrystal.

imer, as expected. The QTAIM of the $CH_3\cdots\pi$ heterodimer is shown in Fig. 7c. Interestingly, three bond CPs and bond path interconnect both molecules. One connects an H-atom of the CH_3 group to the phenanthroline. Moreover, the green RDG isosurface located between the methoxyl group and one ring of the phenantroline confirms the existence of the $CH_3\cdots\pi$ interaction. Another bond CP connects one CH bond of the pterostilbene dimethoxiphenyl ring to one C-atom of the central ring of phenanthroline disclosing the formation of an additional $CH\cdots\pi$ interaction. Finally, a third bond CP connects one O-atom of the methoxy group to the phenanthroline ring, thus suggesting the formation of a $O\cdots\pi$ interaction. The binding energy of this heterodimer is quite modest (–4.9 kcal/mol). Finally, we have computed the tetramers shown in Fig. 7d,e in order to analyze possible cooperativity effects, as suggested by the MEP surface study (previous section). The binding energy of these tetrameric assemblies have been computed as homodimers by considering each pterostilbene/phenanthroline heterodimer as a monomer. By doing so, the energies of the phenanthroline homodimer and those of the tetramers are comparable. Interestingly, the π-stacking energy becomes more negative in both tetramers compared to the homodimer, thus suggesting the existence of cooperativity effects. This reinforcement is related with the reduction of the electrostatic repulsion between the phenanthroline rings, due to an electron transfer from the phenanthroline to the pterostilbene molecules.

4. Conclusions

In summary, this work contributes with new data about cooperativity and interplay of aromatic interactions in the pterostilbene/phenanthroline cocrystal structure, which has been analyzed with a focus on the infrequently dipole-dipole parallel orientation of the aromatic rings of the phenanthroline molecules. DFT calculations disclose that the H-bonds between both coformers facilitate the formation of the face-to-face π-stacked dimers of phenanthroline by reducing the electrostatic repulsion between the π-systems, as corroborated by MEP surface calculations. Moreover, the existence of mutual reinforcement between H-bond and π-

stacking interactions is proposed, based on the energetic and MEP surface analyses. The latter shows that the H-bond acceptor ability of the N-atom of phenanthroline increases upon the formation of the π-stacked homodimer. The energetic study also demonstrates that the OH···N H-bond between both co-formers is the strongest interaction.

Funding

This work was financially supported by the MICIU/AEI of Spain (project PID2020–115637GB-I00 FEDER funds).

Declaration of Competing Interest

The authors declare that they have no known competing financial interests or personal relationships that could have appeared to influence the work reported in this paper

CRediT authorship contribution statement

Rafael Barbas: Data curation, Investigation, Writing – original draft. **Lídia Bofill:** Investigation. **Vineet Kumar:** Investigation. **Rafel Prohens:** Resources, Conceptualization, Validation, Writing – original draft, Writing – review & editing, Supervision. **Antonio Frontera:** Formal analysis, Resources, Conceptualization, Writing – original draft, Writing – review & editing, Supervision.

Data Availability

No data was used for the research described in the article apart from that supplied in the supporting information.

Acknowledgments

We thank Dr. Mercè Font-Bardia (Universitat de Barcelona) for her support with the SCXRD data and also we thank the “centre de tecnologies de la informació” (CTI) at the University of the Balearic Islands for computational facilities.

Supplementary materials

Supplementary material associated with this article can be found, in the online version, at doi:10.1016/j.molstruc.2023.135227.

References

[1] N. Schultheiss, A. Newman, Pharmaceutical Cocrystals and Their Physicochemical Properties, Cryst. Growth Des. 9 (2009) 2950–2967.
[2] D.J. Berry, J.W. Steed, Pharmaceutical cocrystals, salts and multicomponent systems; intermolecular interactions and property based design, Adv. Drug Deliv. Rev. 117 (2017) 3–24.
[3] C.A. Hunter, K.R. Lawson, J. Perkins, C.J. Urch, Aromatic interactions, J. Chem. Soc., Perkin Trans. 2 (2001) 651–669.
[4] S.A. Sharber, W.J. Mullin, S.W. Thomas III, Bridging the Void: halogen Bonding and Aromatic Interactions to Program Luminescence and Electronic Properties of π-Conjugated Materials in the Solid State, Chem. Mater. 33 (2021) 6640–6661.
[5] M. Gallegos, D. Barrena-Espés, J.M. Guevara-Vela, T. Rocha-Rinza, A.M. Pendás, A QCT View of the Interplay between Hydrogen Bonds and Aromaticity in Small CHON Derivatives, Molecules 27 (2022) 6039.
[6] L. Bofill, D. de Sande, R. Barbas, R. Prohens, Hydrogen bond polarization overcomes unfavorable packing in the most stable high Z' polymorph of pterostilbene, Cryst. Growth Des. 19 (2019) 2552–2556.
[7] SADABS Bruker AXS; Madison, Wisconsin, USASAINT, Software Users Guide, Version 6.0; Bruker Analytical X-ray Systems: Madison, WI, 1999. Sheldrick, G. M. SADABS v2.03; Area-Detector Absorption Correction, University of Göttingen, Germany, 2004 1999. Saint, Version 7.60A; Bruker AXS 2008; SADABS, V. 2008-1, 2008.
[8] G.M. Sheldrick, A short history of SHELX, Acta Crystallogr., Sect. A 64 (2008) 112–122.
[9] Gaussian 16, Revision C.01, M.J. Frisch, G.W. Trucks, H.B. Schlegel, G.E. Scuseria, M.A. Robb, J.R. Cheeseman, G. Scalmani, V. Barone, G.A. Petersson, H. Nakatsuji, X. Li, M. Caricato, A.V. Marenich, J. Bloino, B.G. Janesko, R. Gomperts, B. Mennucci, H.P. Hratchian, J.V. Ortiz, A.F. Izmaylov, J.L. Sonnenberg, D. Williams-Young, F. Ding, F. Lipparini, F. Egidi, J. Goings, B. Peng, A. Petrone, T. Henderson, D. Ranasinghe, V.G. Zakrzewski, J. Gao, N. Rega, G. Zheng, W. Liang, M. Hada, M. Ehara, K. Toyota, R. Fukuda, J. Hasegawa, M. Ishida, T. Nakajima, Y. Honda, O. Kitao, H. Nakai, T. Vreven, K. Throssell, J.A. Montgomery, Jr., J.E. Peralta, F. Ogliaro, M.J. Bearpark, J.J. Heyd, E.N. Brothers, K.N. Kudin, V.N. Staroverov, T.A. Keith, R. Kobayashi, J. Normand, K. Raghavachari, A.P. Rendell, J.C. Burant, S.S. Iyengar, J. Tomasi, M. Cossi, J.M. Millam, M. Klene, C. Adamo, R. Cammi, J.W. Ochterski, R.L. Martin, K. Morokuma, O. Farkas, J.B. Foresman, D.J. Fox, Gaussian, Inc., Wallingford CT, 2016.
[10] S. Grimme, J. Antony, S. Ehrlich, H. Krieg, A consistent and accurate ab initio parametrization of density functional dispersion correction (DFT-D) for the 94 elements H-Pu, J. Chem. Phys. 132 (2010) 154104–154118.
[11] F. Weigend, Accurate Coulomb-fitting basis sets for H to Rn, Phys. Chem. Chem. Phys. 8 (2006) 1057–1065.
[12] S.F. Boys, F. Bernardi, The calculation of small molecular interactions by the differences of separate total energies. Some procedures with reduced errors, Mol. Phys. 19 (1970) 553–566.
[13] D. Majumdar, S. Roy, A. Frontera, R.M. Gomila, T.K. Pal, Crystal engineering of Pb (II)-salen coordination polymer enforced for the selective fluorescence NACs sensing activity in a dispersed aqueous medium: a combined experimental and theoretical DFT monologue, J. Mol. Struct. 1276 (2023) 134717.
[14] S. Bhunia, R.M. Gomila, A. Frontera, S. Chattopadhyay, An insight to the role of perchlorate counter ions and different non-covalent interactions in the solid state structures of mono-anionic malonic acid bridged trinuclear mixed valence cationic complexes of cobalt with tetradentate N2O2 donor ligands, Inorg. Chim. Acta 547 (2023) 121324.
[15] D. Dutta, T. Baishya, R.M. Gomila, A. Frontera, M. Barcelo-Oliver, A.K. Verma, M.K. Bhattacharyya, Supramolecular assemblies involving energetically significant unconventional π (CN)-π and anion-π (nitrile) contacts in Zn (II) coordination compounds: antiproliferative and theoretical studies, J. Mol. Struct. 1274 (2023) 134568.
[16] S. Zaib, A. Ibrar, I. Khan, R.M. Gomila, M.U. Tariq, J. Simpson, C.J. McAdam, C.John McAdam, H. Alrbyawi, R.A. Pashameah, E. Alzahrani, A.-E. Farouk, A. Frontera, Unraveling the impact of hydrogen bonding and C–H···π(CN) interactions in crystal engineering of cyclic aminobenzonitriles: a combined X-ray crystallographic and computational Investigation, J. Mol. Struct. 1273 (2023) 134387.
[17] R.F.W. Bader, A bond path: a universal indicator of bonded interactions, J. Phys. Chem. A. 102 (1998) 7314–7323.
[18] T.A. Keith, AIMAII (Version 13.05.06), TK Gristmill Software, Overland Park, KS, 2013.
[19] J. Contreras-García, E.R. Johnson, S. Keinan, R. Chaudret, J.-P. Piquemal, D.N. Beratan, W. Yang, NCIPLOT: a program for plotting noncovalent interaction regions, J. Chem. Theory Comput. 7 (2011) 625–632.
[20] M.A. Spackman, D. Jayatilaka, Hirshfeld surface analysis, CrystEngComm 11 (2009) 19–32.
[21] M.A. Spackman, J.J. Mckinnon, Fingerprinting intermolecular interactions in molecular crystals, CrystEngComm 4 (2002) 378–392.
[22] J.J. Mckinnon, D. Jayatilaka, M.A. Spackman, Towards quantitative analysis of intermolecular interactions with Hirshfeld surfaces, Chem. Commun. (2007) 3814–3816.
[23] P.R. Spackman, M.J. Turner, J.J. McKinnon, S.K. Wolff, D.J. Grimwood, D. Jayatilaka, M.A. Spackman, CrystalExplorer: a program for Hirshfeld surface analysis, visualization and quantitative analysis of molecular crystals, J. Appl. Cryst. 54 (2021) 1006–1011.
[24] M. Harder, B. Kuhn, F. Diederich, Efficient stacking on protein amide fragments, ChemMedChem 8 (2013) 397–404.